Effects of snow, snowmelting and refreezing processes on air–sea-ice CO_2 flux

Daiki NOMURA,[1,2*] Hisayuki YOSHIKAWA-INOUE,[2] Takenobu TOYOTA,[1] Kunio SHIRASAWA[1]

[1]*Institute of Low Temperature Science, Hokkaido University, Sapporo 060-0819, Japan*
E-mail: nomura.daiki@nipr.ac.jp
[2]*Graduate School of Environmental Science and Faculty of Environmental Earth Science, Hokkaido University, Sapporo 060-0810, Japan*

ABSTRACT. The air–sea-ice CO_2 flux was measured in the ice-covered Saroma-ko, a lagoon on the northeastern coast of Hokkaido, Japan, using a chamber technique. The air–sea-ice CO_2 flux ranged from –1.8 to +0.5 mg C m^{-2} h^{-1} (where negative values indicate a sink for atmospheric CO_2). The partial pressure of CO_2 (pCO_2) in the brine of sea ice was substantially lower than that of the atmosphere, primarily because of the influence of the under-ice plume from the Saromabetsu river located in the southeastern part of the lagoon. This suggests that the brine had the ability to take up atmospheric CO_2 into the sea ice. However, the snow deposited over the sea ice and the superimposed ice that formed from snowmelting and refreezing partially blocked CO_2 diffusion, acting as an impermeable medium for CO_2 transfer. Our results suggest that the air–sea-ice CO_2 flux was dependent not only on the difference in pCO_2 between the brine and the overlying air, but also on the status of the ice surface. These results provide the necessary evidence for evaluation of the gas exchange processes in ice-covered seas.

INTRODUCTION

Carbon dioxide (CO_2) is the primary gas involved in the exchange of carbon between ocean and atmosphere. Because sea ice has been assumed to impede the gas exchange between the ocean and atmosphere, the ice-covered areas of the ocean have not been considered important to the air–sea CO_2 flux and the global carbon budget (Tison and others, 2002 and references therein). However, research has shown that when the brine volume fraction is higher than 5% (Golden and others, 1998), sea ice is a permeable medium for CO_2 (Gosink and others, 1976; Nomura and others, 2006). In addition, the partial pressure of CO_2 (pCO_2) in the brine of sea ice becomes supersaturated or undersaturated with respect to the overlying air (e.g. Delille, 2006). It is evident that sea ice can influence the exchange of CO_2 with the atmosphere (Semiletov and others, 2004; Delille, 2006; Nomura and others, 2006).

Sea ice covers ~3–6% of the world's oceans and persists for up to 6 months (Comiso, 2003). During the ice-melting period, uptake of CO_2 by sea ice, which contains brine with a low pCO_2 compared with that of the atmosphere, has been reported in the Arctic and Antarctic Oceans (Semiletov and others, 2004; Delille, 2006; Zemmelink and others, 2006). In contrast, CO_2 is emitted from sea ice to the overlying air when the brine pCO_2 increases with increasing brine salinity (Nomura and others, 2006). These results suggest that the sea-ice formation/melting processes influence the annual global carbon budget (Rysgaard and others, 2007, 2009).

During the entire period of sea-ice cover, various conditions occur on the sea-ice surface: rafting and ridging by dynamic ice-growth processes under turbulent conditions, accumulation of snow deposited over sea ice, snowmelting and refreezing (superimposed ice) and formation of melt ponds in the warmer months of spring and summer (e.g. Perovich, 1998). Measurements of the air–sea-ice CO_2 flux under different sea-ice surface conditions will enable a more complete understanding of the air–sea-ice CO_2 flux. However, there have been few such measurements (Delille, 2006; Zemmelink and others, 2006). In particular, there are no detailed descriptions of the relationships between sea-ice surface conditions and air–sea-ice CO_2 flux.

We examine how snow deposited over sea ice and the processes of snowmelting and refreezing at the ice surface affect the air–sea-ice CO_2 flux. These are important processes to consider when estimating the air–sea-ice CO_2 flux.

MATERIALS AND METHODS

Observation sites

Field observations were carried out in the semi-closed system of Saroma-ko, a lagoon on the Okhotsk Sea coast of Hokkaido, Japan, from 18 February to 9 March 2006 and from 22 February to 4 March 2008 (Fig. 1; Table 1). The surface area of the lagoon is 149.2 km^2 and the mean depth is 14.5 m. Sea ice usually covers almost the entire surface of the lagoon from early January through to early April, with large year-to-year variability (Shirasawa and Leppäranta, 2003). A river-water plume develops under the sea ice in the lagoon as a result of increased discharge of river water during the ice-melt period (Nomura and others, 2009). For this study, we chose six ice stations: one (station main) located ~1.5 km offshore and five others (stations 1–5) forming a transect between the mouth of the Saromabetsu river and the second (east) inlet (Fig. 1; Table 1). For each station, we carried out air–sea-ice CO_2 flux measurements, sampling of sea-ice cores, brine and under-ice water, and ice surface observations. Details of the sampling methods for sea-ice cores, brine and under-ice water, and analytical procedures for physical and chemical properties are given in the Appendix.

*Present address: National Institute of Polar Research, 10-3 Midori-cho, Tachikawa, Tokyo 190-8518, Japan.

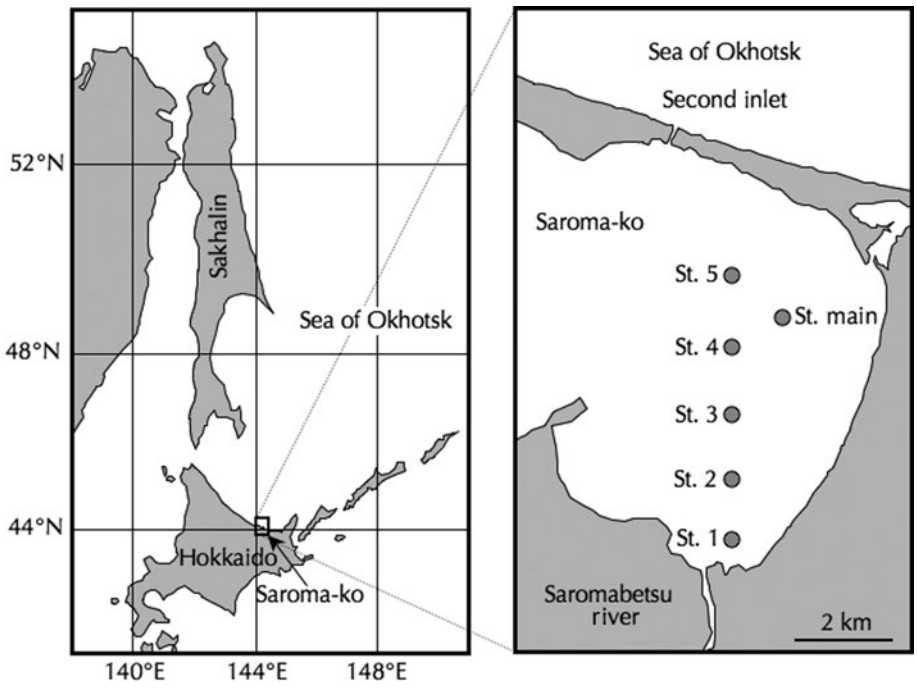

Fig. 1. Locations of sampling stations in Saroma-ko, Hokkaido, Japan: stations 1–5 (44°05.30′–44°07.49′ N, 143°56.59′–143°56.61′ E) and station main (44°07.18′ N, 143°57.34′ E).

Air–sea-ice CO_2 flux measurements

Air–sea-ice CO_2 flux was measured by a closed dynamic chamber method (Fig. 2). This method was used to directly determine CO_2 flux in situ to allow for high spatial resolution. We used a stainless-steel chamber 50 cm in diameter and 30 cm high with a serrated bottom edge to prevent gas from leaking through the chamber–ice interface. The chamber was pushed down firmly into the sea-ice surface to prevent lateral diffusion of CO_2. Sample air from the chamber passed through Teflon tubes connected to a non-dispersive infrared (NDIR) analyzer (GMP343 carbon dioxide probe; Vaisala Ojy, Vantaa, Finland) that was connected to a data logger (RVR 52 data logger; T&D Corp., Nagano, Japan). Temperatures in the chamber were measured during each flux measurement with a temperature sensor (RVR 52 temperature recorder; T&D Corp., Nagano, Japan). The air in the chamber was circulated with a pump at a flow rate of 0.7 L min^{-1} through a mass flow controller and chemical desiccant column containing $Mg(ClO_4)_2$ (Fig. 2). These devices were installed in a portable adiabatic box (40 cm × 25 cm × 30 cm). Electricity was provided by an electric generator. The CO_2 concentration in the chamber was measured every 10 s during experiments lasting 40 min. Four standards (typically 324, 341, 363 and 406 ppm CO_2 in natural air) traceable to the World Meteorological Organization (WMO) mole fraction scale (Yoshikawa-Inoue and Ishii, 2005) were used to calibrate the CO_2-measuring system in the laboratory before the experiment in 2006 and both before and after the experiment in 2008. The instrument drift (output voltage) before and after the experiment for each calibration gas agreed to well within 1%. The CO_2 flux was calculated from the changes in CO_2 concentration in the chamber and the elapsed time (Fig. 3). The precision of the air–sea-ice CO_2 flux from duplicate determination was within ±0.13 mg C m^{-2} h^{-1}.

During the observation period in 2008, the CO_2 flux was measured under two different conditions: (1) a chamber was installed above the sea ice through the snow cover and slush layer deposited over the sea ice (Fig. 4a); and (2) a chamber was installed directly above the sea ice after first removing the snow cover and slush layer with a scoop (Fig. 4b).

Observations of snow cover, slush layer and sea-ice surface conditions

We examined the properties of the snow cover and slush layer deposited over sea ice and determined the condition of the ice surface by measuring the snow thickness and the thickness of the slush layer. We then classified the state of the sea-ice surface into three categories: (1) snow + slush; (2) superimposed ice; and (3) snow + superimposed ice. The temperatures of the air, the air–snow interface, the snow–slush-layer interface and the slush– or snow–sea-ice interface were measured using needle-type temperature sensors (SK-250WP; Sato Keiryoki Mfg. Co., Ltd, Tokyo, Japan).

RESULTS AND DISCUSSION

Properties of snow cover, slush layer, sea ice and sea-ice surface

The properties of the snow cover, slush layer, sea ice and sea-ice surface conditions during our experiments are shown in Table 1. During the observation period in 2006, there was considerable variation in snow thickness and slush-layer thickness. On 18 and 19 February 2006, there were both snow and slush layers on top of the sea-ice surface (Table 1). However, as air temperature increased, the state of the sea-ice surface changed suddenly. From 23 February to 1 March, because of the melting of the snow and the refreezing of the meltwater, the surface of the sea ice was frequently covered by an icy glaze (herein referred to as 'superimposed ice') with neither a snow nor a slush layer (Fig. 5). On 3 March,

Table 1. Sampling dates, locations, properties of snow cover and slush layer over sea ice, ice surface conditions, and sea-ice properties at Saroma-Ko

Date	Station	Snow thickness	Slush layer thickness	Temperature				Sea-ice surface conditions	Ice thickness	Ice temperature		Average brine volume fraction
				Air	Air–snow interface	Snow–slush interface	Snow or slush–ice interface			Surface†	Bottom‡	
		cm	cm	°C	°C	°C	°C		cm	°C	°C	%
2006												
18 February	Main	4.5	8.0	–3.7	–4.3	–2.4	–1.9	snow + slush	38.5	–3.0	–1.8	10.2
19 February	Main	3.0	1.0	–1.8	–1.3	–2.4	–	snow + slush	37.5	–3.1	–1.7	11.6
23 February	Main	0.0	0.0	+0.3	–0.3*	–	–	superimposed ice	38.5	–0.9	–1.8	9.7
23 February	2	0.0	0.0	+0.6	–0.9*	–	–	superimposed ice	43.0	–1.0	–0.8	13.8
24 February	5	0.0	0.0	–	–1.6*	–	–	superimposed ice	47.5	–1.8	–1.9	8.0
24 February	1	0.5	0.0	+1.9	–2.4	–	–	snow + superimposed ice	44.5	–0.8	–0.1	13.0
25 February	Main	0.5	0.0	–2.1	–2.4	–	–	snow + superimposed ice	44.0	–2.3	–1.6	8.5
26 February	4	0.0	0.0	+2.2	–0.8*	–	–	superimposed ice	41.0	–1.5	–1.3	8.5
28 February	3	0.0	0.0	+0.5	–0.9*	–	–	superimposed ice	39.0	–0.4	–0.1	12.4
28 February	Main	0.0	0.0	–3.6	–3.1*	–	–	superimposed ice	36.0	–0.6	–0.8	17.4
1 March	2	0.0	0.0	–1.8	–1.4*	–	–	superimposed ice	46.0	–0.7	–0.6	8.3
3 March	3	16.0	2.0	–3.5	–	–	–0.9	snow + slush	38.0	–0.8	–0.4	7.5
3 March	Main	17.5	6.0	–1.2	–	–	–1.7	snow + slush	32.0	–0.6	–0.4	15.3
4 March	4	16.0	0.0	+0.6	–0.4	–	–0.9	snow + superimposed ice	44.0	–0.5	–0.2	13.5
5 March	5	10.0	0.0	–0.9	–0.9	–	–1.4	snow + superimposed ice	49.5	–0.8	–0.8	8.1
7 March	Main	2.0	0.0	–1.9	–1.9	–	–1.6	snow + superimposed ice	38.5	–0.6	–0.1	13.9
8 March	3	5.0	0.0	–0.8	–0.3	–	–0.8	snow + superimposed ice	45.0	–0.3	–0.4	9.9
9 March	2	6.0	0.0	–0.9	–0.9	–	–0.8	snow + superimposed ice	47.0	–0.3	–0.3	–
2008												
22 February	Main	4.0	3.0	–2.1	–2.3	–3.4	–3.0	snow + slush	41.0	–1.9	–1.1	14.7
23 February	Main	5.5	1.0	–0.8	–1.8	–3.0	–2.8	snow + slush	38.0	–2.8	–1.1	–
25 February	Main	9.5	0.5	–3.7	–6.5	–4.4	–2.9	snow + slush	37.0	–1.0	–1.0	13.7
26 February	Main	19.0	3.0	+1.5	–0.4	–2.9	–2.8	snow + slush	39.0	–1.1	–1.0	12.5
28 February	Main	15.5	0.5	–4.9	–5.0	–3.3	–2.2	snow + slush	46.0	–1.1	–1.0	15.2
29 February	Main	15.5	0.5	+2.0	–	–2.6	–2.5	snow + slush	47.0	–1.0	–1.0	15.9
1 March	Main	12.0	3.0	–2.2	–1.9	–2.8	–2.5	snow + slush	45.0	–1.1	–1.1	11.4
2 March	Main	12.0	11.0	+1.0	–1.5	–1.9	–1.9	snow + slush	46.0	–1.1	–1.1	12.0
3 March	Main	11.0	6.0	–4.2	–4.7	–2.0	–	snow + slush	47.0	–0.9	–1.0	16.2
4 March	Main	12.0	6.0	–0.7	–0.4	–1.1	–	snow + slush	55.0	–1.4	–1.1	13.4

Note: – no data.
*When neither snow nor slush was present, temperatures were measured at the air–icy-surface interface.
†Surface temperature was measured 2–5 cm below the top of the core.
‡Bottom temperature was measured 2–5 cm above the bottom of the core.

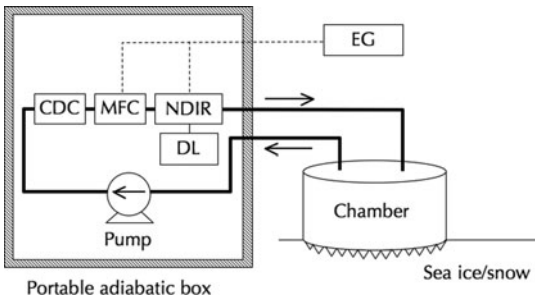

Fig. 2. Schematic diagram of the CO_2-measuring system and stainless-steel chamber. Solid thick lines indicate the closed loop of flowing air for measuring the concentration of CO_2 in the air in the chamber. CDC: chemical desiccant column; MFC: mass flow controller; NDIR: non-dispersive infrared analyser; DL: data logger; EG: electric.

there was >16 cm of snow on top of the superimposed ice. This loading of snow resulted in an upward flushing of water through brine channels in the ice (Hudier and others, 1995), and a slush layer had formed again at station 3 and station main on 3 March. From 4 to 9 March, the snow melted and the snow thickness decreased with time. During this period, there was no slush layer over the sea ice.

During 2008 at station main, snow and slush layers were observed throughout the observation period (Table 1). Snow thickness and slush-layer thickness varied according to the amount of snow deposited over the sea ice and the rate of melting.

The sea-ice thickness was almost constant during each experimental period (Table 1). The ice thickness was 42 ± 5 cm (mean $\pm$ standard deviation) in 2006 and 45 ± 5 cm in 2008. The sea-ice temperature ranged from –3.1°C to –0.1°C in 2006 and from –2.8°C to –0.9°C in 2008 (Table 1). The temperature of sea ice, snow and slush layer increased overall through the experimental period each year (Table 1). These results suggest a transition from the cold

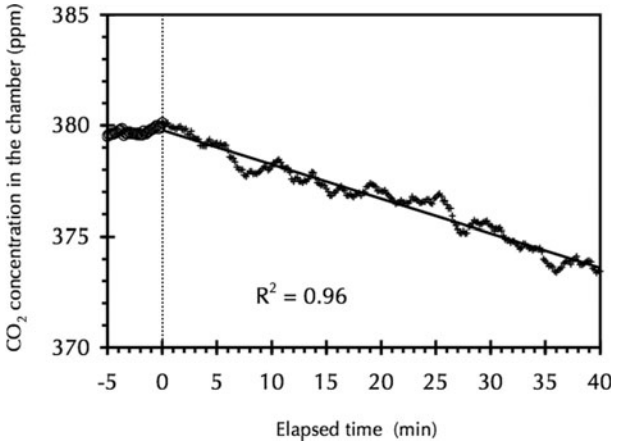

Fig. 3. Example of the temporal variation in CO_2 concentration in the chamber at station main on 29 February 2008 with the condition depicted in Figure 4b (neither snow nor slush). Open circles and crosses reflect the values obtained before and after the measurement, respectively. The regression line is based on the data obtained after the measurement. The vertical dashed line indicates an elapsed time of 0 min.

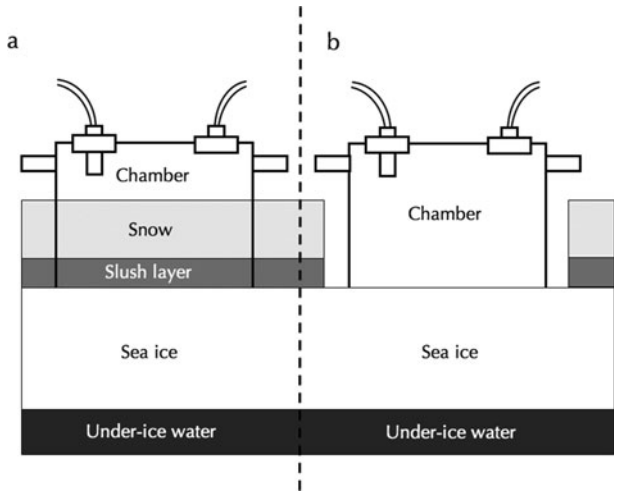

Fig. 4. Schematic diagrams showing two situations for measuring the air–sea-ice CO_2 flux during the 2008 study period in Saroma-ko. (a) The chamber was installed above the sea ice through the snow cover and slush layer deposited over the sea ice. (b) As in (a) but with snow and slush layer removed artificially.

period to the warm or melting period throughout the observation period. The brine volume fraction of sea ice was >5% at all stations (Table 1), indicating that the CO_2 in brine can diffuse through the brine channel (Gosink and others, 1976) due to the high permeability of sea ice (Golden and others, 1998).

Brine pCO_2

The brine pCO_2 is one of the important factors determining the magnitude of the air–sea-ice CO_2 flux (Delille, 2006; Nomura and others, 2006). Here we focus on the distributions of the brine pCO_2 and discuss the mechanisms controlling it.

The brine pCO_2 increased with increasing brine salinity, with a high degree of correlation ($r^2 = 0.86$; $P < 0.05$) (Fig. 6). During the observation period in 2006, both brine salinity and brine pCO_2 spanned wide ranges: 2.3–29.3 for brine salinity and 2.7–195.1 µatm for brine pCO_2. Plots of low

Fig. 5. Photograph of the superimposed ice at station 3 in Saroma-ko on 28 February 2006. The photograph was taken looking west. The length of the standing cores is ~40 cm.

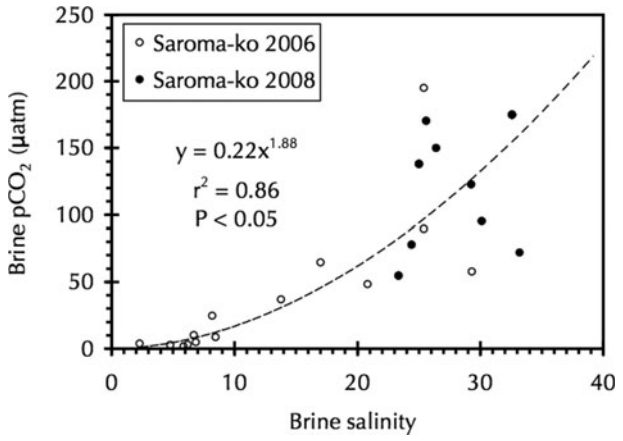

Fig. 6. Relationship between brine salinity and brine pCO_2 during observations in 2006 and 2008. The dashed curve indicates the best fit to describe the relationship ($y = 0.22x^{1.88}$; $r^2 = 0.86$; $P < 0.05$).

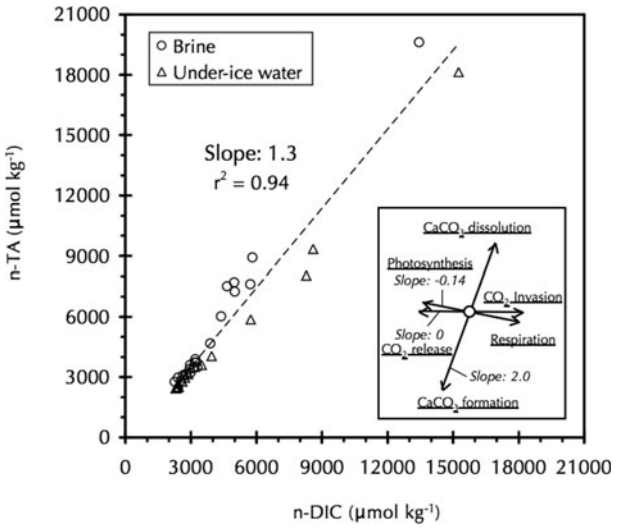

Fig. 8. Relationships between the n-DIC and n-TA (normalized to a constant salinity of 35) for brine and under-ice water during observations in 2006 and 2008. The regression line is based on the brine and under-ice water with slope of 1.3 ($r^2 = 0.94$). The inset indicates the theoretical slope of the different processes affecting n-DIC and n-TA.

brine salinity and low brine pCO_2 corresponded to values observed near the river mouth (stations 1–3) during the entire period and through the transect during the warm period 1–9 March 2006. At station main during the 2006 observations, both brine pCO_2 and brine salinity decreased drastically (Fig. 7). Brine salinity decreased from 38.2 on 19 February to 8.5 on 7 March. Brine pCO_2 decreased from 195.1 µatm on 23 February to 8.6 µatm on 7 March. Near the river mouth (stations 1 and 3) during the 2006 observations, salinity and pCO_2 of under-ice water at 1 m depth below the surface of the sea ice ranged from 3.3 to 18.8 and from 26.1 to 187.2 µatm, respectively. These values are low compared with those of under-ice water at 1 m depth below the surface of the sea ice at station 5 on 5 March 2006 (20.2 for salinity and 320.5 µatm for pCO_2).

During observations in 2008, brine salinity and brine pCO_2 at station main stayed within relatively narrow ranges: 23.3–33.2 for brine salinity and 54.9–175.2 µatm for brine pCO_2 (Fig. 6). In all experiments, brine pCO_2 was undersaturated with respect to the overlying air, with an average value of 388.5 ± 6.1 µatm (mean ± standard deviation) for all observations.

In order to elucidate the process controlling the changes of brine pCO_2, we examine the relationships between the salinity-normalized brine dissolved inorganic carbon (n-DIC) and salinity-normalized total alkalinity (n-TA) (Fig. 8). The samples with low salinity and low pCO_2 for brine and under-ice water exhibit extremely high n-DIC and n-TA when dissolved inorganic carbon (DIC) and total alkalinity (TA) are normalized to a salinity of 35 (Fig. 8). The relationships between n-DIC and n-TA for brine and under-ice water show good agreement ($r^2 = 0.94$). The slope of the regression line for brine and under-ice water is 1.3, and plots of brine and under-ice water are slightly deviated above and below the regression line, respectively.

In Saroma-ko, a salinity and chemical substances (nutrients) gradient has been observed moving offshore from the river mouth (Shirasawa and Leppäranta, 2003; Nomura and others, 2009). Based on the salinity–oxygen-isotopic ratio, the fraction of river water just below the sea ice was estimated to be >80% at stations 2–4 during the warm period of the experiment from 1 to 8 March 2006, whereas the fraction of ice meltwater just below the sea ice was almost zero through the transect during the entire period (Nomura and others, 2009). These results suggest that the changes of n-DIC and n-TA for under-ice water shown in Figure 8 were mainly driven by the effect of the river-water plume developed under the sea ice.

Our study area was located in the southernmost part of the seasonal sea-ice zone in the Northern Hemisphere, where the sea ice is relatively thinner, ice temperature is higher and sea-ice brine volume fraction is higher than in polar seas (Table 1). Water exchange between the well-developed brine channels and under-ice water readily occurred through upward flushing caused by loading of snow deposited over the sea ice (Hudier and others, 1995; Nomura and others, 2009). Therefore, it can be considered that the changes of n-DIC and n-TA for brine were caused by the exchange with under-ice water characterized by the river-water plume under the ice (Fig. 8). At first glance, the slope of the regression line for brine and under-ice water is also close to the theoretical slope for $CaCO_3$

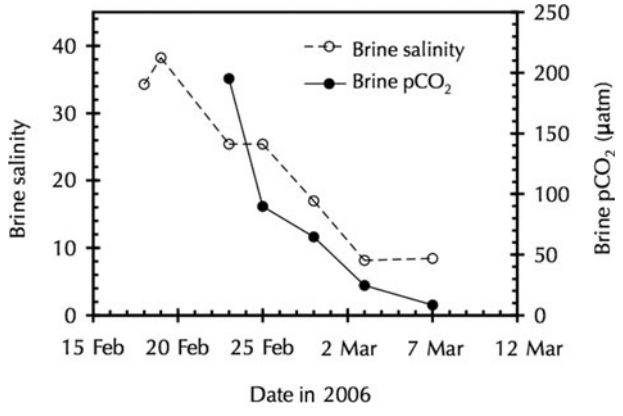

Fig. 7. Changes in brine pCO_2 and brine salinity at station main during observations in 2006.

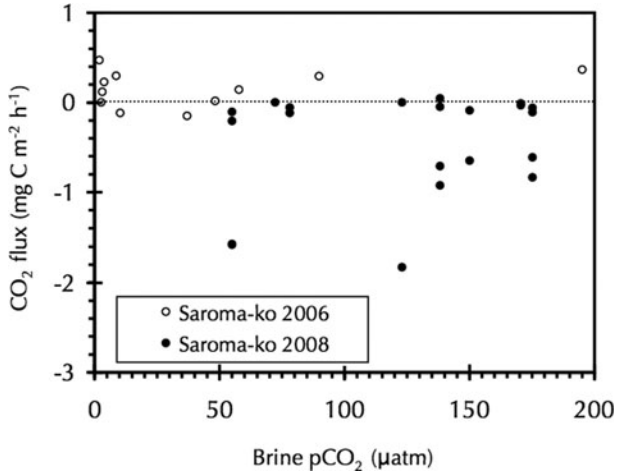

Fig. 9. The air–sea-ice CO_2 flux vs brine pCO_2 for all experiments. The horizontal dotted line indicates an air–sea-ice CO_2 flux of 0 mg C m^{-2} h^{-1}.

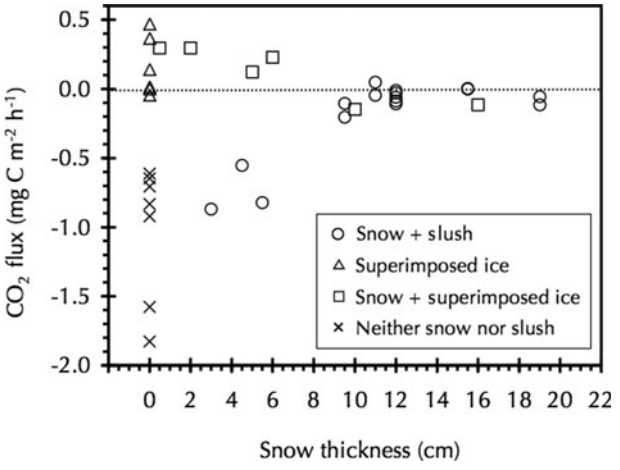

Fig. 10. Relationship between snow thickness and air–sea-ice CO_2 flux for various ice surface conditions. Crosses reflect the conditions depicted in Figure 4b. The horizontal dotted line indicates an air–sea-ice CO_2 flux of 0 mg C m^{-2} h^{-1}.

dissolution (slope = 2.0) (Fig. 8). However, because the high concentration of dissolved inorganic phosphorus in brine (Nomura and others, 2009) and the high ice temperature (Table 1) (compared with the polar seas) impedes the formation of $CaCO_3$ (Killawee and others, 1998; Papadimitriou and others, 2005), we suggest that $CaCO_3$ formation is minimal in sea ice. In addition, in order to demonstrate the wide distributions of n-DIC and n-TA for brine (>10 000 µmol kg^{-1}) (Fig. 8), large quantities of $CaCO_3$ are needed (Delille, 2006). The slight difference between the plots for brine (above the regression line in Fig. 8) and under-ice water (below the regression line) might be attributed to other processes such as photosynthesis. Chlorophyll-*a* concentrations of brine were higher than in under-ice water during our observation period (Nomura and others, 2009). This can lead to the photosynthetic activity of ice algae in brine and depletion of the brine pCO_2 relative to the under-ice water.

Delille (2006) reported that brine pCO_2 changes dramatically from the season of sea-ice formation to the season of melting conditions in the Antarctic pack ice. During sea-ice formation, brine pCO_2 increases with increasing DIC and with changes in CO_2 solubility and the dissociation constants of carbonic acid (Papadimitriou and others, 2003; Nomura and others, 2006). Therefore, brine pCO_2 is supersaturated with respect to the air. On the Antarctic pack ice, the brine pCO_2 increases up to 900 µatm in late winter (Delille, 2006). In contrast, during the ice-melting season, brine pCO_2 becomes undersaturated with respect to the air as a result of the increased net primary production, dilution by melting ice and dissolution of carbonate minerals (Gleitz and others, 1995; Delille, 2006). In Arctic fast ice in spring, brine pCO_2 is 220–280 µatm (Semiletov and others, 2004), and in Antarctic pack ice in summer, brine pCO_2 is about 50 µatm (Delille, 2006).

Air–sea-ice CO_2 flux

The values of the air–sea-ice CO_2 flux obtained in this study ranged from –1.8 to +0.5 mg C m^{-2} h^{-1} (where negative values indicate a sink for atmospheric CO_2) (Fig. 9). The values agree well with the results obtained over bare Antarctic pack ice (–2.6 to +1.0 mg C m^{-2} h^{-1}; Delille, 2006). However, more negative flux values (i.e. increased CO_2 flux from air to sea or water) were observed over melt ponds and open brine channels in the Arctic fast ice (–19.3 to –9.8 mg C m^{-2} h^{-1}; Semiletov and others, 2004) and over snow and slush layers on Antarctic pack ice (–9.1 to –3.3 mg C m^{-2} h^{-1}; Zemmelink and others, 2006), where there is a highly productive ice algae community.

Previous studies report that the air–sea-ice CO_2 flux is mainly influenced by the difference between pCO_2 of the brine in sea ice and that of the overlying air (Delille, 2006; Nomura and others, 2006). We saw during our period of observations that the pCO_2 of the overlying air was almost constant compared with that of the brine. Therefore, the air–sea-ice CO_2 flux will depend primarily on the brine pCO_2. However, in our data there was no clear relationship between the air–sea-ice CO_2 flux and brine pCO_2 when we plotted all the data corrected during the observation period (Fig. 9). These results suggest that there are other processes, in addition to the difference in pCO_2 between the brine and overlying air, that influence the air–sea-ice CO_2 flux. We now examine these other processes.

Relationships between air–sea-ice CO_2 flux and ice surface properties

In order to clarify the process controlling the air–sea-ice CO_2 flux, in addition to the difference of pCO_2 between the brine and overlying air, we examine the relationships between the air–sea-ice CO_2 flux and ice surface properties.

The air–sea-ice CO_2 flux for each ice surface type as a function of the snow thickness is shown in Figure 10 and Table 2. The air–sea-ice CO_2 flux approaches zero with increasing snow thickness for sea-ice surface conditions of snow + slush (Fig. 10). When the snow is deeper than about 9 cm, most of the air–sea-ice CO_2 flux values are near zero (Fig. 10; Table 2). In contrast, when a chamber was installed above the sea ice after first removing the snow and slush layer (Fig. 4b), the negative air–sea-ice CO_2 flux ranged from –1.8 to –0.6 mg C m^{-2} h^{-1} (Fig. 10; Table 2). Even when the snow thickness was less than about 9 cm, the air–sea-ice CO_2 flux values were near zero under conditions where the

Table 2. Air–sea-ice CO_2 flux under different sea-ice surface conditions

Sea-ice surface conditions	Air–sea-ice CO_2 flux mg C m^{-2} h^{-1}
Snow (<9 cm) + slush	–0.9 to –0.6
Snow (>9 cm) + slush	–0.2 to 0.0
Snow + superimposed ice	–0.1 to +0.3
Superimposed ice	0.0 to +0.5
Neither snow nor slush*	–1.8 to –0.6

*See Figure 4b.

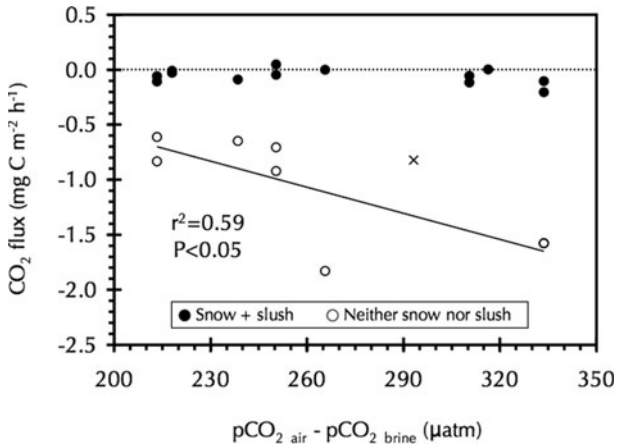

Fig. 11. Relationships between air–sea-ice CO_2 flux and the difference in pCO_2 between the air and the brine in sea ice ($\Delta pCO_{2\_air–brine} = pCO_{2\_air} - pCO_{2\_brine}$) for the two situations depicted in Figure 4 during observations in 2008. Open circles reflect the conditions depicted in Figure 4b. The solid line indicates the linear regression of CO_2 flux vs $\Delta pCO_{2\_air–brine}$ for open circles ($r^2 = 0.59$; $P < 0.05$). The cross indicates the result obtained on 23 February with a snow thickness of 5.5 cm (Table 1). The horizontal dotted line indicates an air–sea-ice CO_2 flux of 0 mg C m^{-2} h^{-1}.

sea-ice surface was classified as snow + superimposed ice or superimposed ice (Fig. 10; Table 2). These results suggest that a superimposed ice surface or a melted snow deposit deeper than 9 cm acts as a physical barrier to CO_2 diffusion from air to sea ice in this area during the ice-melting season, even though the brine in the sea ice has the potential (i.e. relatively low pCO_2) to take up CO_2 from the atmosphere under all ice surface conditions (Fig. 6). These results were coincident with the limited measurement of air–sea-ice CO_2 flux over the superimposed ice in the Antarctic pack ice (Delille, 2006).

We also examined the relationships between the air–sea-ice CO_2 flux and the difference in pCO_2 between the air and brine in sea ice ($pCO_{2\_air} - pCO_{2\ brine} = \Delta pCO_{2\_air–brine}$) for the two situations depicted in Figure 4 (Fig. 11). We found a notable difference between the two situations. When the snow and slush layer were removed artificially (Fig. 4b), there was a clear relationship between the air–sea-ice CO_2 flux and $\Delta pCO_{2\_air–brine}$ ($r^2 = 0.59$; $P < 0.05$), showing that the air–sea-ice CO_2 flux was driven mainly by the difference in pCO_2 between the brine and overlying air (Delille, 2006; Nomura and others, 2006). However, when the air–sea-ice CO_2 flux was measured over the snow cover (>9 cm) and slush layer (Fig. 4a) the flux was near zero.

There are some related studies concerning the air–soil CO_2 flux through snow deposited over soils (Sommerfeld and others, 1993, 1996; Takagi and others, 2005; Schindlbacher and others, 2007). These studies found that the snow cover deposited over soils is a porous medium for gases before snowmelting begins. While CO_2 concentrations in soils drive the overall CO_2 flux through the snow cover, temporal and spatial variability of the CO_2 flux may be caused by specific snowpack properties (Schindlbacher and others, 2007). In particular, during the snowmelting season, because of the meltwater input to the pores in snow (Denoth, 1982), refreezing of meltwater and the formation of a specific ice layer in the snowpack (Schindlbacher and others, 2007), the air–soil CO_2 flux through the snow cover is restricted (Schindlbacher and others, 2007). These same conditions could have occurred in the snow in our experiments because of the relatively high temperatures during our experimental periods (Table 1). Although we have no data regarding the detailed properties of the snow, our results provide direct evidence for the effect of the snow deposited over sea ice on the air–sea-ice CO_2 flux during the ice-melting season. To understand the effects of snow properties on the air–sea-ice CO_2 flux, further investigations are highly desirable to state the snow density, grain shape composition and moisture in more detail.

CONCLUSIONS

We examined effects of snow on sea ice, snowmelting and refreezing processes on air–sea-ice CO_2 flux in the semi-closed lagoon system using a chamber technique. The air–sea-ice CO_2 flux ranged from –1.8 to +0.5 mg C m^{-2} h^{-1} (where negative values indicate a sink for atmospheric CO_2). The partial pressure of CO_2 (pCO_2) in the brine of sea ice was substantially lower than that of the atmosphere, primarily because of the influence of the under-ice plume from the Saromabetsu river located in the southeastern part of the lagoon. The formation of superimposed ice on sea ice and melted snow deposited over sea ice (>9 cm) acted as physical barriers to CO_2 exchange between the air and sea ice even though the brine within the sea ice has the potential to absorb CO_2 from the atmosphere. Our results suggest that the air–sea-ice CO_2 flux is dependent not only on the difference in pCO_2 between the brine and the overlying air but also on the condition of the sea-ice surface, especially during the ice-melting season, indicating that measurements of the air–sea-ice CO_2 flux should also include detailed observations of the sea-ice surface conditions.

Clearly, further investigations will be required to understand the effects of snow properties on the air–sea-ice CO_2 flux and the applicability of the limited results from this study to the general field (e.g. Arctic and Antarctic seas), where the variability in ice surface snow- and ice-melting processes must be an important factor affected by global warming. However, these data provide clues to understanding the evaluation of the gas exchange processes in the ice-covered seas. Indeed, in the Arctic Ocean, formation of superimposed ice early in the melt season is common and has been linked to retention of meltwater at the ice surface in the early stage of melt (Eicken and others, 2004). The overall role of sea ice in the climate system remains to be investigated in other seasonally ice-covered seas (Rysgaard and others, 2007, 2009).

ACKNOWLEDGEMENTS

We thank S. Noriki, H. Hattori, S. Taguchi, S. Aoki, S. Nihashi, Y. W. Watanabe, K. Suzuki, T. Kawamura, M. Ishikawa, T. Takatsuka and Y. Kusumi for sampling assistance, for providing measurement devices and for useful comments. We also thank M. Lange, B. Delille and an anonymous reviewer for useful comments and editorial assistance. This work is partly supported by the Research Fellowship of the Japan Society for the Promotion of Science (#17654098 and #195968).

REFERENCES

Comiso, J.C. 2003. Large-scale characteristics and variability of the global sea ice cover. *In* Thomas, D.N. and G.S. Dieckmann, *eds. Sea ice: an introduction to its physics, chemistry, biology and geology.* Oxford, etc., Blackwell, 112–142.

Cox, G.F.N. and W.F. Weeks. 1983. Equations for determining the gas and brine volumes in sea-ice samples. *J. Glaciol.,* **29**(102), 306–316.

Culberson, C., R.M. Pytkowicz and J.E. Hawley. 1970. Seawater alkalinity determination by the pH method. *J. Mar. Res.,* **28**(1), 15–21.

Delille, B. 2006. Inorganic carbon dynamics and air–ice–sea CO_2 fluxes in the open and coastal waters of the Southern Ocean. (PhD thesis, University of Liège.)

Denoth, A. 1982. The pendular–funicular liquid transition and snow metamorphism. *J. Glaciol.,* **28**(99), 357–364.

Dickson, A.G. 1990. Thermodynamics of the dissociation of boric acid in synthetic seawater from 273.15 to 318.15 K. *Deep-Sea Res. I,* **37**(5), 755–766.

Dickson, A.G. and C. Goyet, *eds.* 1994. *Handbook of methods for the analysis of the various parameters of the carbon dioxide system in sea water, version 2.0.* Oak Ridge, TN, US Department of Energy, Oak Ridge National Laboratory. (ORNL/CDIAC-74.)

Dickson, A.G. and F.J. Millero. 1987. A comparison of the equilibrium constants for the dissociation of carbonic acid in seawater media. *Deep-Sea Res. I,* **34**(10), 1733–1743.

Eicken, H. 2003. From the microscopic, to the macroscopic, to the regional scale: growth, microstructure and properties of sea ice. *In* Thomas, D.N. and G.S. Dieckmann, *eds. Sea ice: an introduction to its physics, chemistry, biology and geology.* Oxford, Blackwel, 22–81.

Eicken, H., T.C. Grenfell, D.K. Perovich, J.A. Richter-Menge and K. Frey. 2004. Hydraulic controls of summer Arctic pack ice albedo. *J. Geophys. Res.,* **109**(C8), C08007. (10.1029/2003JC001989.)

Gleitz, M., M.M.R. van der Loeff, D.N. Thomas, G.S. Dieckmann and F.J. Millero. 1995. Comparison of summer and winter inorganic carbon, oxygen and nutrient concentrations in Antarctic sea ice brine. *Mar. Chem.,* **51**(2), 81–91.

Golden, K.M., S.F. Ackley and V.I. Lytle. 1998. The percolation phase transition in sea ice. *Science,* **282**(5397), 2238–2241.

Gosink, T.A., J.G. Pearson and J.J. Kelley. 1976. Gas movement through sea ice. *Nature,* **263**(5572), 41–42.

Hudier, E.J.J., R.G. Ingram and K. Shirasawa. 1995. Upward flushing of sea water through first year sea ice. *Atmos.–Ocean,* **33**(3), 569–580.

Johnson, K.M., A.E. King and J.M. Sieburth. 1985. Coulometric TCO_2 analyses for marine studies; an introduction. *Mar. Chem.,* **16**(1), 61–82.

Killawee, J.A., I.J. Fairchild, J.L. Tison, L. Janssens and R. Lorrain. 1998. Segregation of solutes and gases in experimental freezing of dilute solutions: implications for natural glacial systems. *Geochim. Cosmochim. Acta,* **62**(23–24), 3637–3655.

Lewis, E. and D.W.R. Wallace. 1998. *Program developed for CO_2 system calculations.* Oak Ridge, TN, US Department of Energy. Oak Ridge National Laboratory. (ORNL/CDIAC-105.)

Mehrbach, C., C.H. Culberson, J.E. Hawley and R.M. Pytkowicz. 1973. Measurement of the apparent dissociation constants of carbonic acid in seawater at atmospheric pressure. *Limnol. Oceanogr.,* **18**(6), 897–907.

Nomura, D., H. Yoshikawa-Inoue and T. Toyota. 2006. The effect of sea-ice growth on air–sea CO_2 flux in a tank experiment. *Tellus B,* **58**(5), 418–426.

Nomura, D., T. Takatsuka, M. Ishikawa, T. Kawamura, K. Shirasawa and H. Yoshikawa-Inoue. 2009. Transport of chemical components in sea ice and under-ice water during melting in the seasonally ice-covered Saroma-ko Lagoon, Hokkaido, Japan. *Estuar. Coast. Shelf Sci.,* **81**(2), 201–209.

Papadimitriou, S., H. Kennedy, G.S. Dieckmann and D.N. Thomas. 2003. Experimental evidence for carbonate precipitation and CO_2 degassing during sea ice formation. *Geochim. Cosmochim. Acta,* **68**(8), 1749–1761.

Papadimitriou, S. *and 6 others.* 2005. Biogeochemical composition of natural sea ice brines from the Weddell Sea during early austral summer. *Limnol. Oceanogr.,* **52**(5), 1809–1823.

Perovich, D.K. 1998. The optical properties of sea ice. *In* Leppäranta, M., *ed. Physics of ice-covered seas.* Helsinki, University of Helsinki Press, 195–230.

Rysgaard, S., R.N. Glud, M.K. Sejr, J. Bendtsen and P.B. Christensen. 2007. Inorganic carbon transport during sea ice growth and decay: a carbon pump in polar seas. *J. Geophys. Res.,* **112**(C3), C03016. (10.1029/2006JC003572.)

Rysgaard, S., J. Bendtsen, L.T. Pedersen, H. Ramløv and R.N. Glud. 2009. Increased CO uptake due to sea ice growth and decay in the Nordic Seas. *J. Geophys. Res.,* **114**(C9), C09011. (10.1029/2008JC005088.)

Schindlbacher, A., S. Zechmeister-Boltenstern, G. Glatzel and R. Jandl. 2007. Winter soil respiration from an Austrian mountain forest. *Agric. Forest Meteorol.,* **146**(3–4), 205–215.

Semiletov, I., A. Makshtas, S.-I. Akasofu and E.L. Andreas. 2004. Atmospheric CO balance: the role of Arctic sea ice. *Geophys. Res. Lett.,* **31**(5), L05121. (10.1029/2003GL017996.)

Shirasawa, K. and M. Leppäranta. 2003. Hydrometeorological and sea ice conditions in Saroma-ko lagoon, Hokkaido, Japan. *Rep. Ser. Geophys.* 46, 161–168.

Sommerfeld, R.A., A.R. Mosier and R.C. Musselman. 1993. CO_2, CH_4 and N_2O flux through a Wyoming snowpack and implications for global budgets. *Nature,* **361**(6408), 140–142.

Sommerfeld, R.A., W.J. Massman, R.C. Musselman and A.R. Mosier. 1996. Diffusional flux of CO_2 through snow: spatial and temporal variability among Alpine–subalpine sites. *Global Biogeochem. Cycles,* **10**(3), 473–482.

Takagi, K. *and 8 others.* 2005. Dynamic carbon dioxide exchange through snowpack by wind-driven mass transfer in a conifer–broadleaf mixed forest in northernmost Japan. *Global Biogeochem. Cycles,* **19**(GB2), GB2012. (10.1029/2004GB002272.)

Tison, J.L., C. Haas, M.M. Gowing, S. Sleewaegen and A. Bernard. 2002. Tank study of physico-chemical controls on gas content and composition during growth of young sea ice. *J. Glaciol.,* **48**(161), 177–191.

Wakita, M., S. Watanabe, Y.W. Watanabe, T. Ono, N. Tsurushima and S. Tsunogai. 2005. Temporal change of dissolved inorganic carbon in the subsurface water at Station KNOT (44°N, 155°E) in the Western North Pacific subpolar region. *J. Oceanogr.,* **61**(1), 129–139.

Weiss, R.F. and B.A. Price. 1980. Nitrous oxide solubility in water and seawater. *Mar. Chem.,* **8**(4), 347–359.

Yoshikawa-Inoue, H. and M. Ishii. 2005. Variations and trends of CO_2 in the surface seawater in the Southern Ocean south of Australia between 1969 and 2002. *Tellus B,* **57**(1), 58–69.

Zemmelink, H.J., B. Delille, J.L. Tison, E.J. Hintsa, L. Houghton and J.W.H. Dacey. 2006. CO_2 deposition over the multi-year ice of the western Weddell Sea. *Geophys. Res. Lett.,* **33**(13), L13606. (10.1029/2006GL026320.)

APPENDIX

Methods for sampling sea-ice cores, brine and under-ice water

Sea-ice cores were collected with a SIPRE-type (US Army Snow, Ice and Permafrost Research Establishment) ice corer with an inner diameter of 7.5 cm. Immediately after ice cores were collected the ice-core length was measured using a ruler, and temperatures were measured by inserting a needle-type temperature sensor (SK-250WP; Sato Keiryoki Mfg. Co., Ltd, Tokyo, Japan) into holes drilled into the core. The ice cores were placed in a polythene bag and stored horizontally in a cooler along with snow to maintain low temperatures and to minimize brine drainage from sea-ice cores. Thereafter, the ice cores were transported to the Saroma Research Center for Aquaculture and stored in a freezer at –30°C. The ice cores were later analysed to determine ice bulk salinity and to estimate the brine volume fraction of the sea ice.

Samples of the sea-ice brine were collected by the gravity drainage method. Full details of this technique are presented by Nomura and others (2009). The brine collected into 200 mL sample bottles was divided into subsamples: one in a 10 mL glass vial for measuring salinity and one in a 120 mL glass vial for measuring brine DIC and brine TA. Mercuric chloride ($HgCl_2$; 50 µL) was added to the DIC sample to stop biological activity.

Under-ice water samples were collected through the ice-core holes using a 500 mL Teflon water sampler (GL Science Inc., Tokyo, Japan) at 1 m depth below the surface of the sea ice. These water samples were collected approximately 15 min after drilling the ice cores, in order to avoid any effects from the disturbance caused by drilling. The under-ice water samples were stored in the same manner as the brine samples for further analysis.

Sample analysis

Salinity of the brine and under-ice water samples was measured using a salt analyser (SAT-210; Toa Electronics Ltd, Tokyo, Japan). The standard deviation for salinity calculated from 15 subsamples taken from a reference water sample ($S = 10.00$) was 0.03 (Nomura and others, 2006). DIC was determined by coulometry (Johnson and others, 1985). DIC measurements were calibrated with working sea-water standards traceable to the Certified Reference Material distributed by A.G. Dickson (Scripps Institution of Oceanography, La Jolla, California, USA). The precision of DIC analysis from duplicate determinations was within ±0.1% (Wakita and others, 2005). TA was analysed by the improved single-point titration method (Culberson and others, 1970). We measured TA using a glass electrode calibrated with Tris buffer and 2-aminopyridine buffer (Dickson and Goyet, 1994). The precision of the TA analysis from duplicate determinations was within ±0.2% (Wakita and others, 2005). The pCO_2 of brine and under-ice water were computed from DIC and TA using the computer program CO2SYS, version 01.05 (Lewis and Wallace, 1998). We used the carbonate dissociation constants (K_1 and K_2) of Mehrbach and others (1973) as refit by Dickson and Millero (1987), and the K_{SO4} determined by Dickson (1990). Air pCO_2 was calculated from air CO_2 concentration by assuming a barometric pressure of 1 atm and saturated water vapour of brine (Weiss and Price, 1980).

For estimation of the brine volume fraction, the ice-core sample was cut to a 4.5 cm × 2.5 cm rectangular cross-section with a bandsaw and then sliced into 3 cm thick sections in the cold room at –15°C. The bulk volume and mass of the 3 cm thick sea-ice sections were measured to calculate the density of the sea ice. The sea-ice sections were then melted to measure salinity, and finally the brine volume fraction of sea ice was calculated with the equations of Cox and Weeks (1983) and Eicken (2003). The brine volume fraction can be derived as:

$$F_b \equiv V_b/V = (\rho S_i)/(\rho_b S_b), \quad \text{(A1)}$$

where V_b is the brine volume, V is the sea-ice bulk volume, ρ is the sea-ice bulk density and S_i is the salinity after melting. In a temperature range higher than –23°C, brine salinity, S_b, and density, ρ_b (g cm^{-3}), as a function of sea-ice temperature and salinity can be approximated by the following:

$$\rho_b = 1 + 8 \times 10^{-4} S_b \quad \text{(A2)}$$

$$S_b = [1 - (54.11/T)]^{-1} \times 1000 \quad \text{(A3)}$$

where T is the temperature (°C).

MS received 27 April 2009 and accepted in revised form 1 February 2010